



Faculty of Medicine of the University of Coimbra
Integrated Master in Dentistry

**Comparative evaluation of two superstructures used for passivity
tests on implant-supported prosthesis: a pilot study**

Ana Júlia da Fonseca Mendes Eiras Branquinho

Supervisor: Prof. Doutor Pedro Miguel Gomes Nicolau

Co-Supervisor: Doutor Nuno Miguel da Silva Tavares Sampaio

Coimbra, 2016

Comparative evaluation of two superstructures used for passivity tests on implant-supported prosthesis: a pilot study

Branquinho AJ¹, Sampaio N², Nicolau P³

1. Student of the Integrated Master in Dentistry of the Faculty of Medicine of the University of Coimbra
2. Assistant Lecturer of the Integrated Master in Dentistry of the Faculty of Medicine of the University of Coimbra
3. Auxiliar Professor of the Integrated Master in Dentistry of the Faculty of Medicine of the University of Coimbra

Department of Dentistry, Faculty of Medicine, University of Coimbra

Av. Bissaya Barreto, Blocos de Celas

3000-075 Coimbra, Portugal

Tel: +351 239 484 183

Fax: +351 239 402 910

E-mail: julia.branquinho@hotmail.com

Acknowledgements

I want to thank my family, specially my parents, my brothers and my grandparents for unconditional love and support, wisdom sharing and having enough patience to deal with me in the hardest times.

I would also like to express my gratitude towards my supervisor Prof. Doutor Pedro Miguel Gomes Nicolau and co-supervisor Dr. Nuno Miguel da Silva Tavares Sampaio, for all the help, dedication, knowledge sharing and precious advice.

Also, I am very grateful to Dra. Tânia Alexandra Correia Rodrigues Baiôa for her collaboration, availability and indispensable help to this study.

Furthermore, I am grateful to the prosthetics laboratory Laboratório Técnico-Dentário, lda., (Coimbra, Portugal) for providing the material used in this study.

I would like to thank all my colleagues, who became my friends, with whom I shared the last 5 years of my life, especially Joana and Bárbara for the countless moments we shared. And my friends for always being there by my side, for all the unforgettable stories, humor, constant support, indispensable friendship and precious memories to come for the next many many decades.

Finally, I would like to thank all the professors that inspired me to learn and always push myself further, thank you all.

Abstract:

Introduction: In an implant-supported prosthesis, passivity should be considered the prime requisite, so a good and long-lasting mechanical stability and implant osseointegration can be guaranteed. The presence of total passivity is still a theoretical termination, once several distortions can occur in the fabrication stages of implant-supported prosthesis. This characteristic can be determined by clinical evaluation or more objective evaluation methods, using computational, analytical and experimental models. Recent studies have used Digital Image Correlation (DIC) for measuring micro-movements and surface strain distribution in implant-supported prosthesis. Our pilot study aims to evaluate the micro-movements and strain distribution on a stone superstructure (SS) and a resin superstructure (RS), on an implant-supported prosthesis, during pre-load torque, using the method of 3D Digital Image Correlation (DIC-3D).

Materials and Methods: Three Screw-Line ConeLog® conical implants were embedded in acrylic resin and a Dual-phase one-step impression was made, to obtain a master cast. SS and RS were fabricated in the laboratory over the master cast and passivity was evaluated, at 10 and 20 N, with a hex screw driver connected to the torque wrench, using 3 methods: (1) Direct visual evaluation and applying the Sheffield Test; (2) Radiographic evaluation; (3) 3-D Digital Image Correlation (DIC-3D) and the software Vic-Snap 2010 and Vic-3D 2012.

Results: Through direct visualization, Sheffield Test and radiographic evaluation, SS and RS were considered to have acceptable clinical passivity. In the DIC-3D evaluation, SS and RS show similar patterns of micro-movement in the U, V and W components and similar Von Mises strain distribution. For all three components, RS shows higher minimum and maximum values of micro-movement. In the U component, the highest values of micro-movement registered for SS and RS are the micro-movements in the right direction.

Conclusions: Both superstructures exhibit similar patterns of micro-movement and Von Mises strain distribution, in the DIC-3D evaluation. The followed tightening sequence influenced the micro-movement and Von Mises strain distribution. The higher values registered for RS are due to several physical properties, and comparing to SS, RS seems to be a worse superstructure for passivity tests.

Keywords: Implant-supported prosthesis, passivity, superstructure, micro-movements, Von Mises strain, 3D Digital Image Correlation

Resumo

Introdução: Numa reabilitação implanto-suportada, a passividade deve ser considerada um requisito primordial para que haja uma duradoura estabilidade mecânica e a osteointegração seja garantida. A presença de total passividade continua a ser um termo teórico, pois podem surgir distorções ao longo das várias fases deste tipo de reabilitação. Esta característica pode ser determinada clinicamente ou recorrendo a métodos mais objectivos, através de modelos computacionais, analíticos e experimentais. Estudos recentes utilizam a Correlação de Imagem Digital (CID) para medição do deslocamento e distribuição de tensões na superfície de uma prótese implanto-suportada. O nosso estudo piloto tem como objectivo avaliar os micro-movimentos e distribuição de tensões numa sobreestrutura de gesso (SG) e numa de resina (SR), durante a pré-carga de torque, utilizando a Correlação de Imagem Digital 3D (CID-3D).

Materiais e Métodos: Três implantes cónicos Screw-Line ConeLog® foram incluídos em resina acrílica e uma impressão Dual-phase de um passo foi realizada para se obter o modelo de trabalho. SG e SR foram fabricadas no laboratório sobre o modelo de trabalho e a passividade foi avaliada, aos 10 e 20N, com uma chave hexagonal conectada à chave de torque, utilizando 3 métodos: (1) Visualização directa e aplicação do Teste de Sheffield; (2) Avaliação radiográfica; (3) Correlação de Imagem 3D (CID-3D) e softwares Vic-Snap 2010 e Vic-3D 2012.

Resultados: Através de visualização directa, Teste de Sheffield e avaliação radiográfica, SG e SR foram consideradas como clinicamente aceitáveis em termos de passividade. Na avaliação com CID-3D, SG e SR mostram padrões semelhantes de micro-movimentos nos componentes U, V e W e padrões semelhantes de distribuição de tensões de Von Mises. Em todos os componentes, SR apresenta valores mínimos e máximos de micro-movimento mais elevados. No componente U, os valores mais altos de micro-movimento para SG e SR foram os movimentos na direcção para a direita.

Conclusões: Ambas as sobreestruturas apresentam padrões semelhantes de micro-movimento e distribuição de tensões de Von Mises, através da avaliação com CID-3D. A sequência de apertos efectuada influenciou os micro-movimentos e distribuição de tensões de Von Mises. Os valores mais elevados registados para SR devem-se a várias propriedades físicas e, comparando com SG, SR aparenta ser uma sobreestrutura menos adequada para testes de passividade.

Palavras-chave: Prótese implanto-suportada, passividade, sobreestrutura, micro-movimentos, tensões de Von Mises, Correlação de Imagem 3D

Index

Introduction7
Materials and Methods.....13
Results.....21
Discussion28
Conclusions35
Appendix
 • List of Figures.....36
 • List of Tables.....38
 • List of Abbreviations39
Bibliographic References40

Introduction

Oral rehabilitation using implant-supported prosthesis aims to reestablish the patient's function and aesthetics, without compromising bone and periodontal health. There are several factors that should be taken into account when rehabilitating such patients: passivity a good occlusion; and the utilization of biocompatible materials (1). Passivity intended as the simultaneous circumferential contact on the entire seating surface of the prosthesis with the implants (2).

Contrasting with natural teeth and alveolar bone connection, implant-alveolar bone interface does not possess periodontal ligament, which makes this junction more rigid (3). In fact, osseointegrated implant shows a range of movement limited to 10 μ m, while in natural teeth the existence of periodontal ligament provides a movement up to 100 μ m, thus atoning for a certain lack of precision that exists in a rehabilitation using implant-supported prosthesis (4). Therefore, an implant shows much lower range of movement, being dependent on bone elasticity modulus, which is influenced by bone density, showing interpersonal variability (2).

The lack of flexibility of bone-implant interface causes direct transmission of all the strength from prosthesis to the alveolar bone (3) because there is no periodontal ligament to absorb a fraction of the load. Thus it is important that the load is transmitted to the remaining bone in a way similar to the physiological transmission that previously existed, once magnitude variations and distribution of such load will have a negative impact on stress quantity and quality to which the set implant-prosthesis-bone is subjected (5).

Therefore, if the implant-supported prosthesis does not show passivity, being mal-adapted, tensile forces (compression and flexure) are generated causing various problems, such as: fracture or loss of implant screws, or even bone (6), an eventual fracture of the prosthesis (3), the appearance of micro-fractures on the periimplant bone (2) and reduction of assembly stability (7).

Actually biomechanical factors inherent to this rehabilitation choice are of great importance, once they are responsible for the longevity and clinical success of this therapy (5).

Thus, in a rehabilitation using implant-supported prosthesis passivity should be considered as the prime requisite, so a good and long-lasting mechanical stability and implant osseointegration can be guaranteed (8). This osseointegration is due to the existence of a biological tolerance, in other words: the ability that the bone surrounding the implants has to cope with the stresses distributed along the implant-bone interface, without occurring clinical complications (9).

For 30 years, several techniques have been successfully used in the rehabilitation of patients with implant-supported prosthesis, although, literature suggests that total passivity is yet to be achieved (6), though there is no consensus.

In fact, various studies tried to numerically quantify the level of acceptable misfit at the implant-abutment interface, but, again, no consensus was found (9).

Branemark was the first to quantify passive fit, stating that it should be as low as 10 μ m, in order to allow bone remodeling and maturation in response to occlusal forces, however values this low are difficult to obtain clinically (1).

Also on this matter, it was proposed by Jemt, that a vertical discrepancy of approximately 150 μ m would be considered clinically acceptable, once it does not represent long-term negative effects (10), this value corresponds to approximately half a screw turn (11). Other studies refer that it is clinically unacceptable the presence of a discrepancy superior to 30 μ m in over 10% of the circumference of the implant (12).

It is reported that higher discrepancy values do not necessarily imply higher incidence of biological complications (1), but there is no consensus when it comes to the relation between the two entities, being the literature quite contradictory in this topic (13).

Due to the great diversity of terms used to describe microgaps detected at the implant-abutment interface, Kano et al. came up with a classification system, based on the horizontal and vertical gap dimensions: (a) type I, no vertical or horizontal gap; (b) type II, existence of horizontal microgap; (c) type III, presence of vertical microgap; and (d) type IV, presence of horizontal and vertical microgap (2).

The presence of total passivity is still a theoretical termination, it cannot be clinically applicable in oral rehabilitation with implant-supported prosthesis, once several distortions can occur in its fabrication stages (3), causing misfit appearance.

The term distortion is used to identify relative movement of one point or several points away from an originally specified referent position, occurring permanent deformation (14).

Such distortions show a multi-dimensional pattern (11) and can be the result of various laboratory or clinical stages, being related to several rehabilitation aspects, such as: impression technique chosen, impression material and quantity used, accuracy of the transfer impression technique, design, fabrication and welding of the substructure (2), execution of the study model, finishing and insertion of the prosthesis (15) and clinician's experience (2).

The deformation present can lead to posterior failure of the components, once we cannot account for the physiologic compensation mechanisms that exist in natural bone, and screw tightening only leads to the disguise of the pre-existent stress (11). Therefore, these clinical and laboratorial stages must be eliminated, minimized or compensated, with the purpose of obtaining well-adjusted implant-supported prosthesis (15).

Prior making well-adjusted implant-supported prosthesis, passive fit test superstructures are usually made to assure accuracy of implants on stone models relatively to the 3D actual intraoral localization of those implants. These discrepancies can be detected by various methods, and are usually the same used to check passive fit of final prosthesis.

Passivity is a characteristic that can be determined by clinical evaluation, visually or using a microscope (13). Clinical evaluation should be based on three aspects: final tightening of prosthetic screw less than 120 degrees, absence of pain or stress during prosthetic insertion and visual analysis using magnifying glasses or radiographs during structure adjustment by manual tightening of the screws (2).

Kan et al. recommended several clinical evaluation methods, proposing that they should be combined in order to achieve objective results and increase their reliability (9). The methods proposed include:

Alternate finger pressure, detecting rocking or saliva movements at the implant-abutment interface; direct vision and tactile sensation, using an explorer (this technique is limited by the size of the explorer, approximately 60 microns); radiographic evaluation, which depends on the angulation; screw resistance test, which consists in tightening the screws one by one until the initial resistance was met in one of the screws, starting with the implant closest to the midline and if it was necessary to tighten that screw more than extra half turn in order to achieve the ideal screw seating, it meant that the framework presented misfit; use of disclosing material, such as fit checker, disclosing wax and pressure indicating paste at the interface; dimensional quantifying systems, that can be used intra-orally (3-D photogrammetric) or extra-orally (coordinate measuring machine); lastly Sheffield Test, which involves tightening one terminal screw and observing the displacement generated in the opposite side (9).

In fact, the use of this last clinical method (Sheffield Test) is vastly recommended for the assessment of clinical fit and it appears to show great sensibility in detecting rotational displacement that induce the lift of opposing cylinders (11).

Ideally, direct clinical evaluation would be preferred, however this methods have several limitations, such as: ethical issues, evaluation for long periods of time, difficult methodology (once direct clinical evaluation of infra-osseous structures is almost impossible) (5) and also the difficulty in detecting small discrepancies (13).

In order to overcome these limitations (5), more objective evaluation methods appeared throughout the last three decades (13), using computational, analytical and experimental models resorting to Finite Element Analysis (FEM), Photoelasticity, Strain Gauges (5), Optical Scan Analysis (13), Reflex Microscopy (11), Scanning Electron Microscopic Analysis (SEM) (15) and Stereomicroscope (16). Several studies have shown that these analysis methods are complementary (5).

The Finite Element Method (FEM) consists in the division of the element-problem into many smaller and simpler elements, creating a mesh of elements and enabling their resolution with mathematical functions (5).

Using 2 or 3-dimensional mechanical models, FEM allows researchers to apply different loadings and obtain stress and displacement measure on tooth, prosthesis, implant and bone, extrapolating the results obtained in *in vitro* studies into *in vivo* situations (5).

However, this analysis method has its disadvantages and limitations: the construction of very complex models, necessity to adopt simplifications and assumptions when it comes to bone quality (homogeneous and isotropic) and bone-implant interface, which can represent several repercussions in final results (5).

Photoelastic analysis is based on the color change, resulting from refraction indices alteration (or optical anisotropy) of certain plastic materials when subjected to stress/deformation, using photoelastic models that can be measured and photographed. Photographic data is qualitatively analyzed in order to investigate the propagation and intensity of stress. This way, the clinician is able to visualize stress patterns in complex structures, such as oral structures, making it possible to localize and quantify stress magnitude (5).

Goiato et al. stated that Photoelastic analyses can be 2-dimensional, 3-dimensional or quasi-3-dimensional (Photoelastic model is 3-dimensional but the fringes are observed 2-dimensionally (5).

This method has some limitations such as the fact that this is an indirect method and requires similar patterns of reproduction to be compared with clinical situations. Additionally, the limit of applied external force may exceed the limit of resistance of the Photoelastic material, which could change the outcome or promote material rupture. Lastly, although the resin used in this technique has an elasticity modulus similar to bone tissue, there is no differentiation between cortical and trabecular bone, which will alter the magnitude of stress induced by the load (5).

Concerning Strain Gauges, these are small electric resistors that detect, measure, calculate and record deformation of the object to which they are connected, when it is subjected to stress, altering the resistance created in their current. The captured electrical signal is sent to a data acquisition board, then modified into a digital signal and interpreted by a computer (5).

The relationship between electrical current and force is determined using a force inducer connected to each cylinder of the superstructure. This instrument converts the electrical current (volts) measured by the strain gauges into force (Newton), allowing the researcher to determine the amount of misfit and calculate forces after connecting to the superstructure (13).

When it comes to the ideal model for this technique: some state that strain gauge should be placed directly on prosthetic pieces, while others defend it should be placed on similar bone materials, in this matter, measurements are restricted to where the gauge is embedded or bounded (5).

Since the Strain Gauge technique is a numerical method, the assumptions necessary makes it imperative to check its accuracy, however, it is considered a reliable method and some authors use it associated to photoelasticity or FEM (5).

In a study conducted by Mitha et al., a different evaluation method was chosen, using Reflex Microscope (Reflex Measurement), which allows a highly precise and tri-dimensional assessment of casting distortion. This was done by measuring distances in the wax framework and its casting between a set of reference pins: 3 external pins, 3 horizontal and 3 vertical (11).

Tahmaseb et al. uses yet another method: Optical Scanning, recurring to an industrial optical scanner and high precision scan adaptors mounted on the implants, in order to calculate implants' position (13).

In this in vitro study, in which the first method was compared with the strain gauge method in the precise assessment of fit, the author concluded that both successfully detected a known misfit and also a single inaccurate implant connection on an implant superstructure. Furthermore, Optical scanning proved to be simpler, more precise and less time consuming than the Strain Gauge method, having value as a quality control measure in dentistry (13).

Another study used Stereomicroscopic analysis to evaluate marginal adaptation of 3-unit cement-retained implant-supported fixed dental prosthesis, when three different torque values were adopted. This analysis was made by measuring the vertical margin gap in three pre-determined reference points (mid-buccal, mid-lingual and mid-lateral side of each abutment) (16).

Recent studies have yet used another method for evaluating passivity in implant-supported prosthesis: Digital Image Correlation (DIC) (17, 18). DIC is a non-contact (19) optical method that has been used for measuring micro-movements (19) and surface strain distribution in materials' testing (18).

This method allows direct-assessment to micro-movements of the object in study (17) and provides a full-field strain measurement of its surface, being more accurate than the existing manual measurement methods. DIC works by tracking blocks of pixels in digital photographs of the object in study at different stages of deformation and establishing comparison (19).

To the present date, no method is considered the ideal one. All the techniques used to evaluate passivity have their vantages and limitations, and in order to decrease their limitations, there is consensus amongst researches that all methods are complementary. Therefore, these methodologies can be applied in the field of Dentistry, guiding further research and clinical studies by predicting some possible disadvantages and rationalizing clinical time (5).

Our pilot study aims to evaluate the micro-movements and strain distribution on a stone superstructure (SS) and a resin superstructure (RS), during pre-load torque, using the method of 3D Digital Image Correlation (DIC-3D).

Materials and Methods

Three Screw-Line ConeLog® implants (Camlog, Maybachstrasse, Germany) were used for our study, two 4.3x13 conical implants and one 3.8x13 conical implant.

For the inclusion of the three implants, a plastic transparent rectangular box was the mold to fix in the middle of a metallic support, using a silicone index made of Virtual XD Putty Fast Set (Ivoclar Vivadent®, Schaan, Liechtenstein) to maintain it in place.

The implants were placed in the following position (from left to right): 4.3x13mm Screw-Line ConeLog® implant (Camlog, Maybachstrasse, Germany) (Implant 1); 4.3x13mm Screw-Line ConeLog® implant (Camlog, Maybachstrasse, Germany) (Implant 2); and 3.8x13mm Screw-Line ConeLog® implant (Camlog, Maybachstrasse, Germany) (Implant 3).

The three conical implants were maintained parallel and evenly spaced, >3mm apart, using two metallic rulers (Figure 1) and then embedded in acrylic resin Ivoclar ProBase Cold (Ivoclar Vivadent®, Schaan, Liechtenstein), the mixture of the resin components was made in six increments, in order to control polymerization contraction and avoid pores inside the resin matrix (Figure 2).

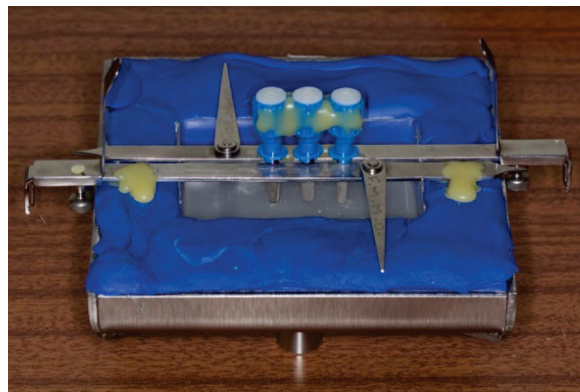


Figure1. Implants maintained in place using two metallic rulers.

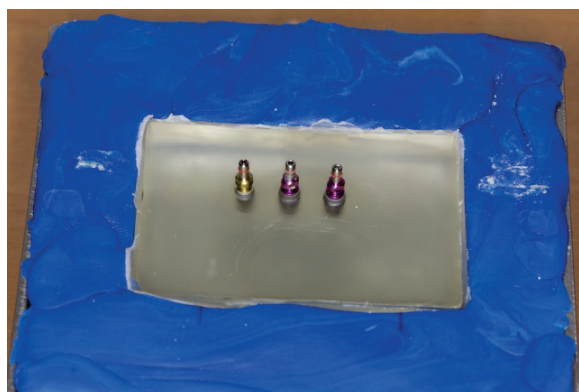


Figure2. Implants embedded in acrylic resin.

A Dual-phase one-step impression was made using two silicones, Virtual Light Body Fast Set (Ivoclar Vivadent®, Schaan, Liechtenstein) and Virtual Putty Fast Set (Ivoclar Vivadent®, Schaan, Liechtenstein), and ConeLog® Impression Posts (Camlog, Maybachstrasse, Germany) and ConeLog® Impression Caps (Camlog, Maybachstrasse, Germany) for the closed tray technique (Figure 3).

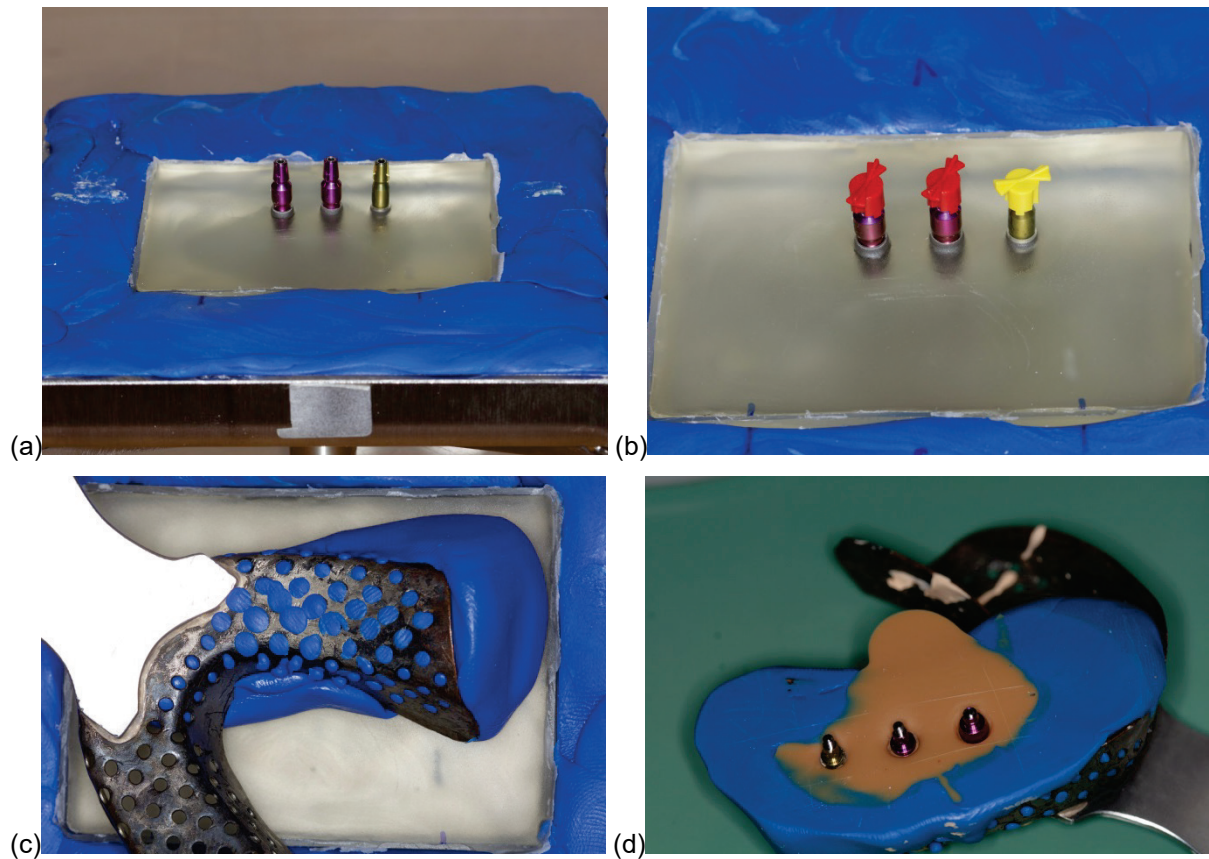


Figure3. Dual-phase one-step closed tray impression technique used. **(a)** Implants with the Impression posts; **(b)** Impression caps attached to the insertion posts; **(c)** Closed tray with the two silicones; **(d)** Final result of the impression technique with the retrieved impression caps and impression posts.

After this step, a prosthetics laboratory (Laboratório Técnico-Dentário, Ida., Coimbra, Portugal) was instructed to construct a master cast in gypsum die GC Fujirock® EP type IV (GC America Inc., Illinois, USA) (Figure 4) and two superstructures, using the adequate Guide System ConeLog® Insertion Posts (Camlog, Maybachstrasse, Germany): a stone superstructure (SS) made in a gypsum die GC Fujirock® EP type IV (GC America Inc., Illinois, USA) (SS), as seen in Figure 5, and a resin superstructure (RS) made in self-curing acrylic resin Pattern Resin™ LS (GC America Inc., Illinois, USA).

The properties and characteristics of the materials used in this pilot study are summarized in table I.

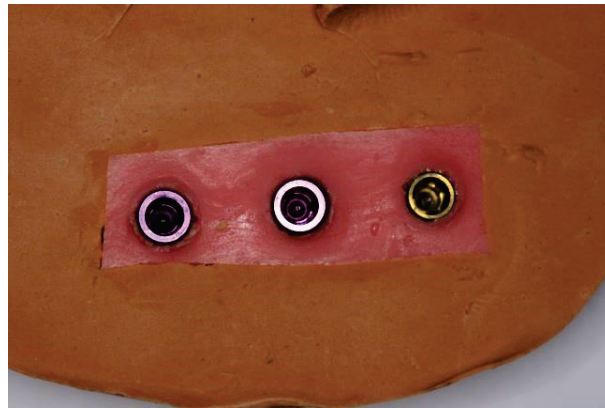


Figure4. Master cast, fabricated in the laboratory.

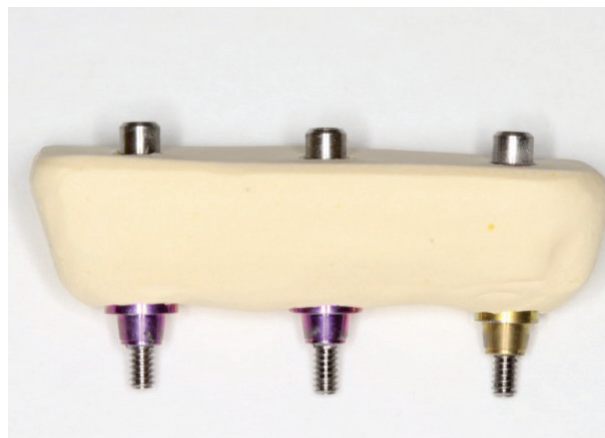





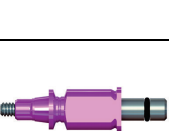




Figure5. Stone superstructure (SS) fabricated in the laboratory.

Table I. Characterization of the implants, impression copings, impression caps, insertion posts and implant analogues used. All the material produced by Camlog, Maybachstrasse, Germany.

		Type	Dimensions	Characteristics	Reference	Material
Implant		Screw-Line ConeLog® Promote® Plus	3.8x13mm	Implant-abutment connection with self-locking cone geometry; Integrated platform switching	C1062.3813	Titanium Grade 4
			4.3x13mm		C1062.4313	
Impression Coping And Impression Cap		Screw-Line ConeLog®	3.8mm	Closed tray Impression	C2110.3800 J2111.3800	Ti-6Al-4V Grade 5 POM
			4.3mm		C2110.4300 J2111.4300	
Insertion Post And Insertion Pin		Guide System ConeLog®	3.8mm		C2026.3800	Ti-6Al-4V Grade 5
			4.3mm		C2026.4300	
Implant Analogues		ConeLog® Lab Analogs	3.8x13mm		C3010.3800	Titanium Alloy
			4.3x13mm		C3010.4300	

In both superstructures, passivity was evaluated using 3 methods: (1) Direct visual evaluation and applying the Sheffield Test; (2) Radiographic evaluation; (3) 3-D Digital Image Correlation (DIC-3D).

First, for the direct visual evaluation, SS and RS were manually connected to the master cast and all three insertion posts were tightened until a slight resistance was felt and then untightened, in order to verify if there was resistance to the passive fit of all the superstructure. This approach was repeated for both SS and RS connected to the acrylic block.

Photographs were taken of the two superstructures connected to the master cast and acrylic block, to confirm if passive fit was present. First, SS and RS were photographed when passively connected to the acrylic block, that is with all three insertion posts untightened (Figures 6 and 7), then, photographs were taken of both superstructures connected to the master cast and acrylic block, this time will all three insertion posts manually tightened until a slight resistance was felt.

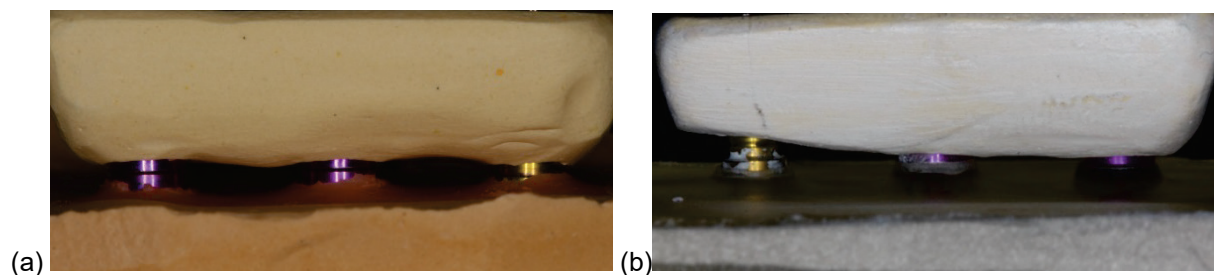


Figure6. SS with all three insertion posts untightened. **(a)** Connected to the master cast; **(b)** Connected to the acrylic block.

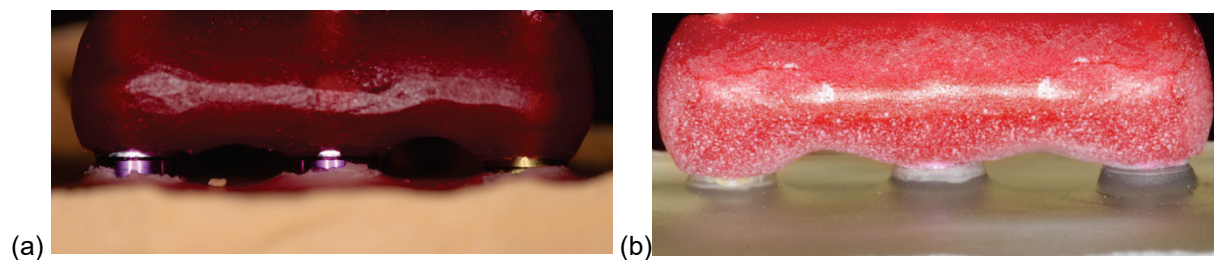


Figure7. RS with all three insertion posts untightened. **(a)** Connected to the master cast; **(b)** Connected to the acrylic block.

Magnifying loupes Kepler Kompakt 3,5x (ExamVision, Samso, Denmark) were used to check for any discrepancy between the implants and insertion posts of SS and RS connected to the master cast and acrylic block.

Using the Sheffield Test, for each superstructure, the terminal 4.3mm insertion post (insertion post n.1) was manually tightened until resistance was felt, while the 4.3mm middle (insertion post n.2) insertion post and the 3.8mm terminal insertion post (insertion post n.3)

were loosened. The displacement generated in the opposite side of the tightened insertion post was observed for SS and RS.

Secondly, radiographs were taken using a ORIX-AET X-ray machine (ARDET Dental & Medical Devices S.r.l., Milan, Italy), with a radiation dose of 0,4mV/0,5s, in a closed chamber, using the reusable phosphor plates CS 7600 Smart Plate Size 2 (31x41mm) (Carestream Health Inc., NY, USA) and a paralleling technique, in order to visualize without distortion both sides of the implant spirals. The phosphor plates were scanned using the CS 7600 (Carestream Health Inc., NY, USA), processed with the Kodak Dental Imaging Software 6.12.32.0 (Carestream Health Inc., NY, USA) and saved in a JPEG.format.

Radiographs were taken first of SS after manually screwing the superstructure to the implants embedded in the acrylic block and tightening them just until a slight resistance was felt. Three radiographs were taken of the superstructure: S1 X-ray with insertion post tightened on implant in position 1 (4.3 Ø, proximal end position) and the other two untightened; S2 X-ray with insertion post tightened on implant in position 2 (4.3 Ø, middle position) fully tightened and the other two untightened; S3 X-ray with insertion posts tightened on all implants (Figure 8).

Afterwards, the same procedure was done with the RS as shown in Figure 9 of radiographs R1, R2 and R3, respectively.

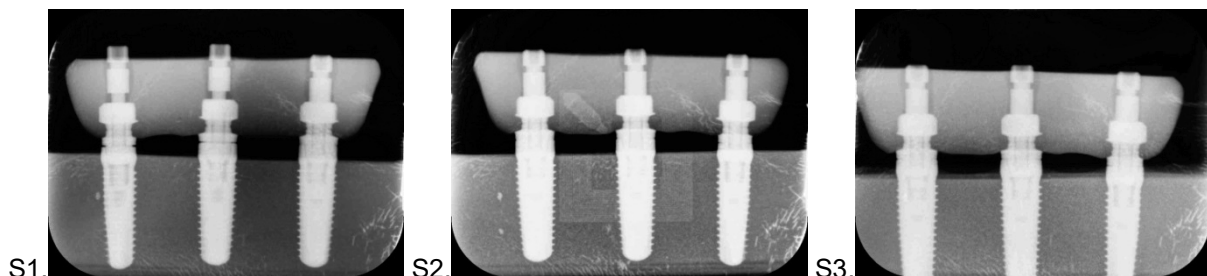


Figure8. Radiographs of SS after manually screwing the superstructure to the implants embedded in the acrylic block.

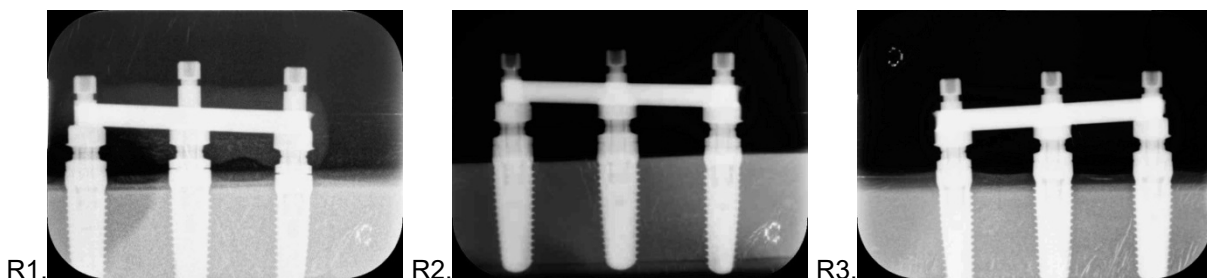


Figure9. Radiographs of RS after manually screwing the superstructure to the implants embedded in the acrylic block.

Then, a software for Image Processing and Analysis in Java, ImageJ (National Institutes of Health, Bethesda, Maryland, USA), was used to measure the microgap present in radiographs S1 and R1 for the SS and RS, respectively.

Finally, evaluation using 3D Digital Image Correlation (DIC-3D) took place. For this procedure, SS and RS were both hand-sprayed with opaque white paint and then air-sprayed with black paint using the Airbrush Pro-Color (Harder & Steenbeck, D22851, Norderstedt, Germany), as seen in Figure 10. This step aimed to produce a non-repetitive, isotropic speckle pattern on the surface of the superstructures that would optimize their analyses using DIC-3D and Vic-3D 2012 (Correlated Solutions®, Columbia, SC, USA).

Each superstructure was assembled to the implants embedded in the acrylic resin block using the ConeLog® short hex screw driver (Camlog, Maybachstrasse, Germany), to manually tighten each Guide System ConeLog® Insertion Posts (Camlog, Maybachstrasse, Germany) just until a slight resistance was felt.

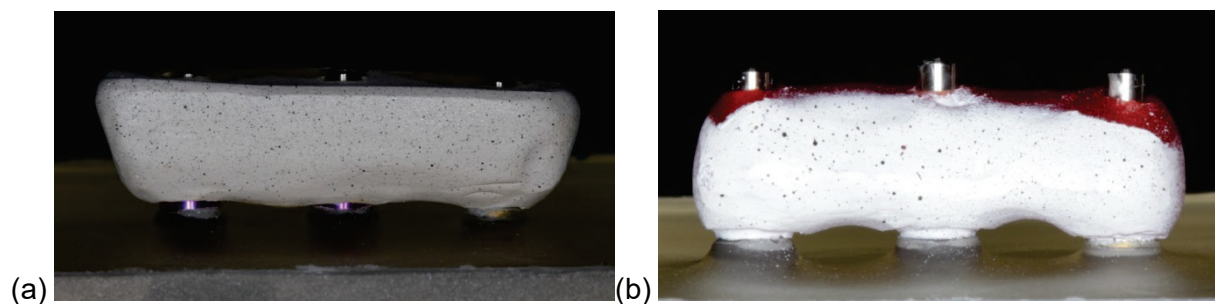


Figure 10. Superstructures hand-sprayed with opaque white paint and air-sprayed with black paint using the Airbrush Pro-Color. **(a)** SS; **(b)** RS.

Using the hex screw driver connected to the torque wrench, both superstructures were then submitted to increasing torque values, by tightening each one of the insertion posts with torques of 10N and 20N. The tightening procedure followed the same order for SS and RS at all torque values: the respective insertion posts were tightened first on implant 1, then on implant 2 and finally on implant 3.

For all the torque values applied to the SS and RS, micro-movements were captured with two high-speed photographic cameras (Stingray F504B ASG, Allied Vision Technologies, LENS 75mm with an extension tube of 5 mm, 0,7:11, Correlated Solutions®, Columbia, USA) at the maximum resolution of 1624x1224 pixels, assembled according to the manufacturer's indications. The two cameras were positioned symmetrically and in a manner to obtain an angle of 15°-45° with the assembly in study, magnification was maintained constant and an illumination source, with adequate potency, was directed to the study model.

The captured speckle images were evaluated using the software Vic-Snap 2010 and Vic-3D 2012 (Correlated Solutions®, Columbia, SC, USA).

A dot grid was used for the calibration of the stereo system, light was adjusted, when necessary, and then the dot grid was photographed simultaneously by both cameras while being rotated into several positions in the three axes of space (V, vertical; U, lateral; and W, antero-posterior). The calibration allows the construction of an algorithm that can correlate deformation detected on both superstructures with micro-movement. The final score is established in pixels and the lower the score the more accurate is the algorithm.

In our study, stereo system calibration was performed using a 4-in-1 Calibration Target (Grid A, size 14.929mm, pitch 1.780, 9x9) for SS, and a 1 inch Calibration Target (size 9x9, pitch 3mm) for RS.

An area on the surface of each superstructure was defined, as well as a single point to be analyzed by the software Vic-3D 2012 and the calibration correspondent to each test was introduced.

Also, rigid body movement of the assembly (acrylic resin block) was removed using the average transformation algorithm. This method calculates the average deformation for the acrylic resin block and inverts it to obtain an image with an average micro-movement of 0 for that surface, therefore reflecting only the SS and RS micro-movements in the V, U and W transformed axes of space.

The speckle images obtained were analyzed by Vic 3D 2012, allowing the formation and evaluation of a 3D representative image of the micro-movements and strain distribution of SS and RS during the increasing pre-load torques on the V, U and W components.

For each sample (SS and RS), minimum and maximum values of micro-movement of the superstructure surface were collected at 10N and 20N, for each insertion post, in the three axis of space. Minimum and maximum values of Von Mises strains and their distribution over the defined areas were also collected.

Results

Through visualization, using magnifying loupes, of both superstructures connected to the implants embedded in the acrylic block or to the master cast, no visible gap between insertion posts and implants or implant analogs, respectively, was detected. Therefore SS and RS were considered to have acceptable clinical passivity (Figures 6 and 7).

Using the Sheffield Test, no displacement of either SS or RS was detected while lightly tightening the insertion post into the implant in position n.1 and loosening the other two. So, both superstructures were considered to have acceptable clinical fit using this method of evaluation.

Radiographically, for SS and RS, a microgap is detected only on radiographs S1 and R1, respectively, in which the insertion post on the proximal end position is lightly tightened and the other two insertion posts are loosened.

Using the software Image Processing and Analysis in Java, ImageJ (National Institutes of Health, Bethesda, Maryland, USA), the values of the microgaps measured in these radiographs were: 99 μ m for SS and 67 μ m for RS.

However, both superstructures are considered to have clinically acceptable passive fit, since the evaluated implant system has an internal conical connection and the detected discrepancy appears to be lower than 150 μ m (6).

On radiographs S2 and R2, where only the middle insertion post was tightened and radiographs S3 and R3, where all insertion posts were tightened, no microgap is detected for both superstructures.

Concerning DIC-3D analyses, for both specimens in study, values of micro-movement were recorded in micrometers (μ m) during tightening of each implant insertion post at 10N and 20N. The minimum and maximum values of micro-movement in U, V and W transformed axes are summarized in Table II.

Lateral or mesio-distal movements were interpreted as micro-movements in the U component, positive values represent micro-movement of the superstructure to the right side of the cameras, while negative values represent micro-movement to the left.

The vertical or coronal-apical movements were interpreted as micro-movement in the V component, maximum values represent micro-movements of the superstructure in the upwards direction, while minimum values represent micro-movements in the downwards direction.

In the W component, antero-posterior or vestibule-lingual/palatine movements were recorded, positive values were interpreted as micro-movements towards the set of cameras and negative values as micro-movements away from the set of cameras.

In Table II, it is registered that SS showed inferior minimum and maximum values of micro-movement when compared to RS, for all the directions interpreted (U, V and W) and torque values.

Regarding the SS, for the U component, higher micro-movement values ($-2.85\mu\text{m}$ and $+3.30\mu\text{m}$) were registered during tightening of the middle insertion post (on implant n.2) with a torque value of 10N. For the V component, using the same torque, higher vertical micro-movement values were also registered during tightening of the same insertion post and in the upwards direction ($+4.95\mu\text{m}$), while, for a torque of 20N, greater micro-movement values were recorded during tightening of insertion post n.1.

For SS, the overall higher micro-movement values were registered in the W component. Greater antero-posterior micro-movement values were recorded during tightening of insertion post n.3, for 10N. While, for 20N torque, the greater micro-movement was registered when tightening insertion post n.1.

Concerning the RS, for both U and V components, micro-movements were higher while tightening insertion post n.2, for both 10N and 20N, while in the W component, micro-movement values were greater during tightening insertion post n.3, for 10N and insertion post n.1, for 20N.

Table II: Minimum and maximum values of micro-movement of SS and RS in the lateral (U), vertical (V) and antero-posterior (W) directions according to the torque applied to each implant insertion post. Individual values are expressed in micrometers (μm).

		U		V		W			
		Left	Right	Downwards	Upwards	Forwards	Towards		
10 N	SS	1	-1.11	+1.25	-1.50	+2.02	-4.46	+4.35	
		2	-2.85	+3.30	-3.55	+4.95	-4.80	+5.30	
		3	-2.32	+1.76	-2.08	+2.32	-5.30	+5.60	
	RS	1	-1.40	+1.26	-1.34	+1.80	-6.40	+5.60	
		2	-3.90	+6.70	-9.50	+10.00	-6.40	+6.20	
		3	-3.40	+6.40	-3.60	+5.85	-7.40	+7.20	
	20 N	SS	1	-1.70	+1.66	-2.60	+2.10	-4.90	+5.55
			2	-1.72	+1.68	-1.70	+1.96	-4.75	+5.30
			3	-1.76	+1.56	-1.76	+1.84	-4.75	+4.90
RS		1	-3.15	+5.05	-3.55	+5.25	-8.20	+7.10	
		2	-3.70	+5.65	-3.95	+6.60	-7.00	+7.20	
		3	-3.40	+5.45	-3.80	+5.80	-7.10	+7.00	

Representative images of the Vic-3D allowed the comparison of SS and RS for the micro-movements suffered in the components U, V and W. For that comparison the images chosen were the representative images of the Vic-3D in which the insertion post n.2 is being tightened with a torque value of 10N.

In the U component, the superstructures present a similar pattern of lateral micro-movements as it is seen in Figure 11, with a tendency for no lateral micro-movements in the area of insertion post n.2.

In the RS, the micro-movement to the right (+6.70 μ m) is almost double of the one to the left (-3.90 μ m), while in the SS the opposite micro-movements do not show a great difference between them (+3.30 μ m and -2.85 μ m).

Also, RS shows values of lateral micro-movements almost double of those of SS and the highest values of micro-movement registered for both superstructures are always the micro-movements in the right direction.

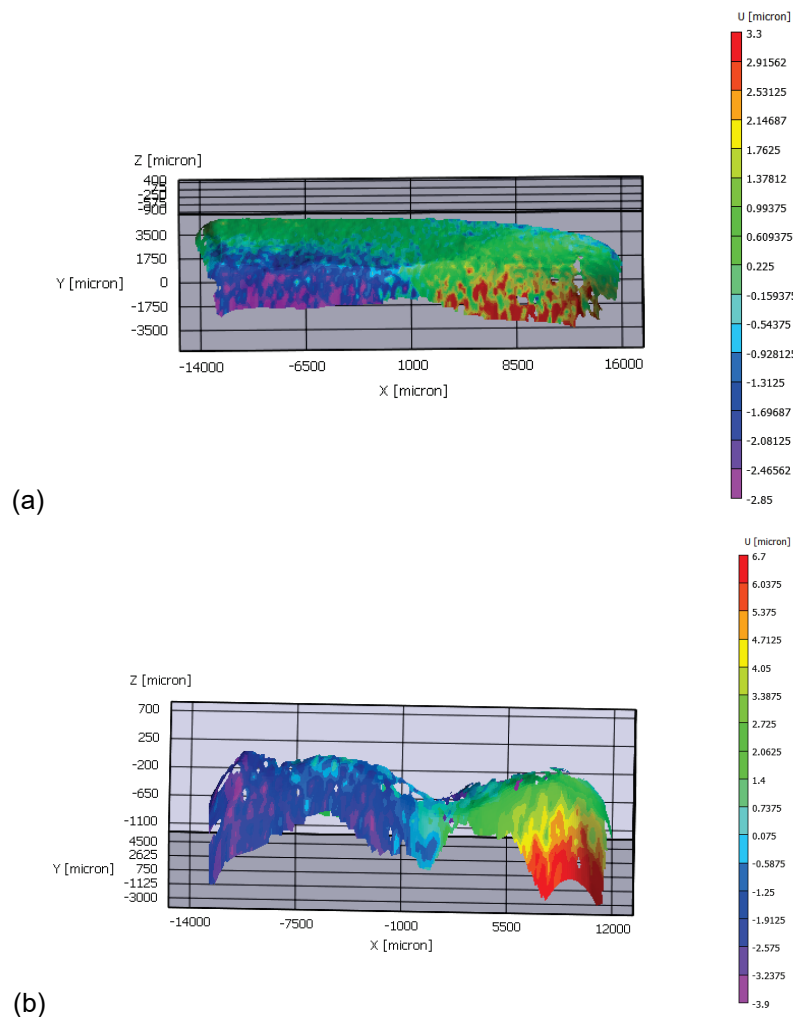


Figure11. Representative image of the Vic-3D output for the micro-movements of the superstructures, considered the fixed rigid body removal, for the U direction, during tightening of implant post n.2 with a torque value of 10N; (a) SS; (b) RS.

Concerning the vertical micro-movements interpreted in the V direction, SS and RS show again similar pattern of micro-movements. As it is seen in Figure 12, the pattern is almost symmetrical: the extremities of the superstructures tend to move upwards and the right extremity shows more micro-movement; in the area of insertion posts n.1 and 3 there is no micro-movement; and in the central area the superstructures tend to move downwards.

In SS, micro-movement in the downwards direction is about 70% lower than the micro-movements in the upwards direction, while for RS the opposite micro-movements have almost the same value ($-9.50\mu\text{m}$ and $+10.00\mu\text{m}$).

Again, the RS shows higher values of vertical micro-movements than SS.

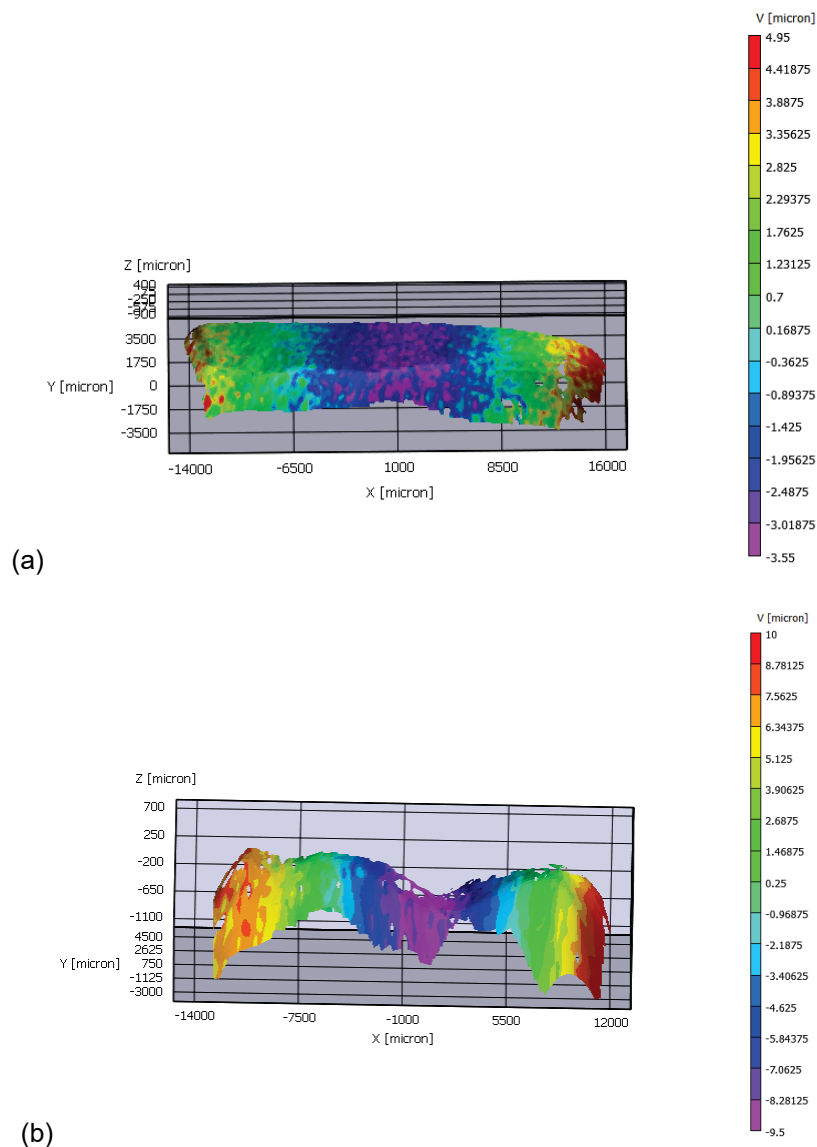


Figure12. Representative image of the Vic-3D output for the micro-movements of the superstructures, considered the fixed rigid body removal, for the V direction, during tightening of implant post n.2 with a torque value of 10N; **(a)** SS; **(b)** RS.

In the W direction, both superstructures show a very heterogeneous pattern of antero-posterior micro-movement, with the majority of micro-movements occurring in the inferior region of SS and RS (close to the insertion posts) and extremities.

For SS, minimum and maximum values are similar. The inferior region of the superstructure tends to move towards the set of cameras, while the extremities tend to move away from the set of cameras, as it is seen in Figure 13(a).

For RS, the left side of the superstructure and the right extremity tend to move towards the cameras, while the area of insertion post n.2 tends to move away from the cameras, as it is seen in Figure 13(b).

Once again, RS shows greater values of antero-posterior micro-movement than SS, but with a lower difference when comparing to the U and V components.

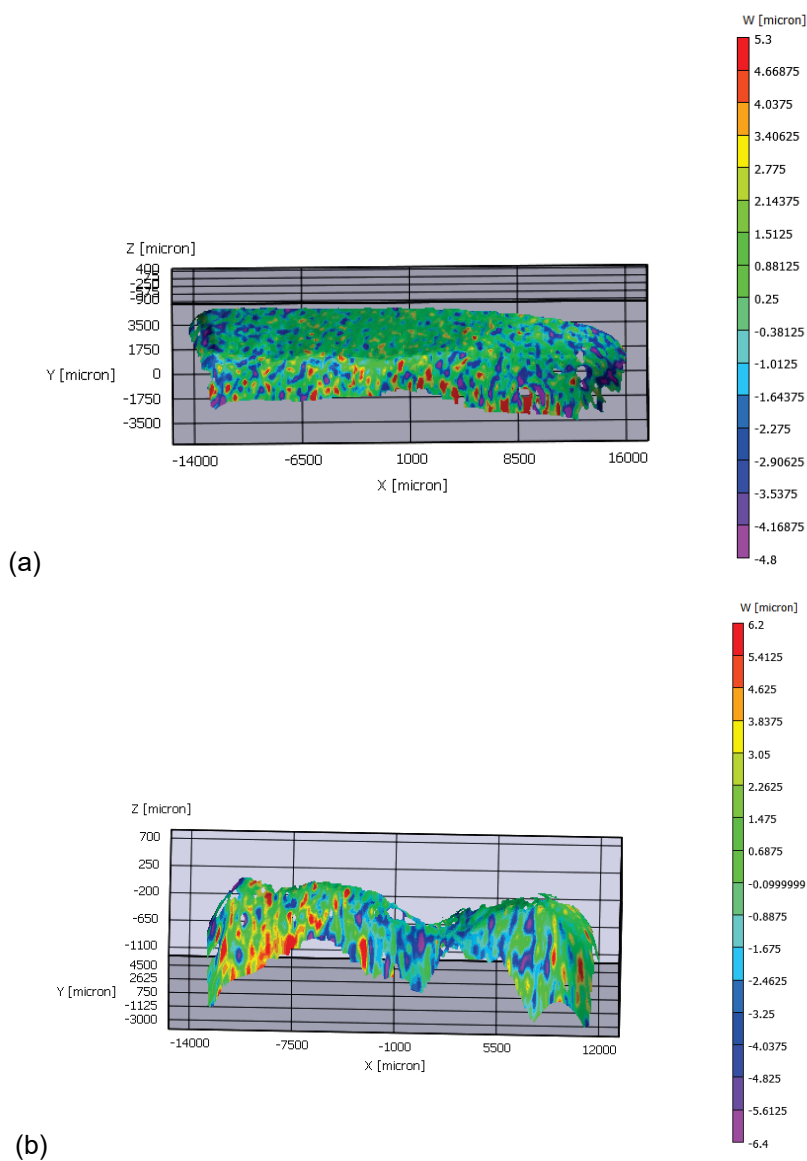


Figure13. Representative image of the Vic-3D output for the micro-movements of the superstructures, considered the fixed rigid body removal, for the W direction, during tightening of implant post n. 2 with a torque value of 10N; **(a)** SS; **(b)** RS.

In the Von Mises strain distribution, a measure of the global geometric deformation taking place at each point of the surface is represented in Figure 14.

For SS, the strain distribution appears to be homogeneous, with a tendency for accumulating tension in the inferior region, area of the substructure around the neck of insertion posts and extremities of the superstructure.

For RS, the strain distribution also has a homogeneous appearance, with a tendency for accumulating tension in the inferior regions between the insertion posts and the area of the neck of the insertion posts.

RS shows higher values of Von Mises Strain, than SS, and the strain values found on the superior region of both superstructures tend to zero.

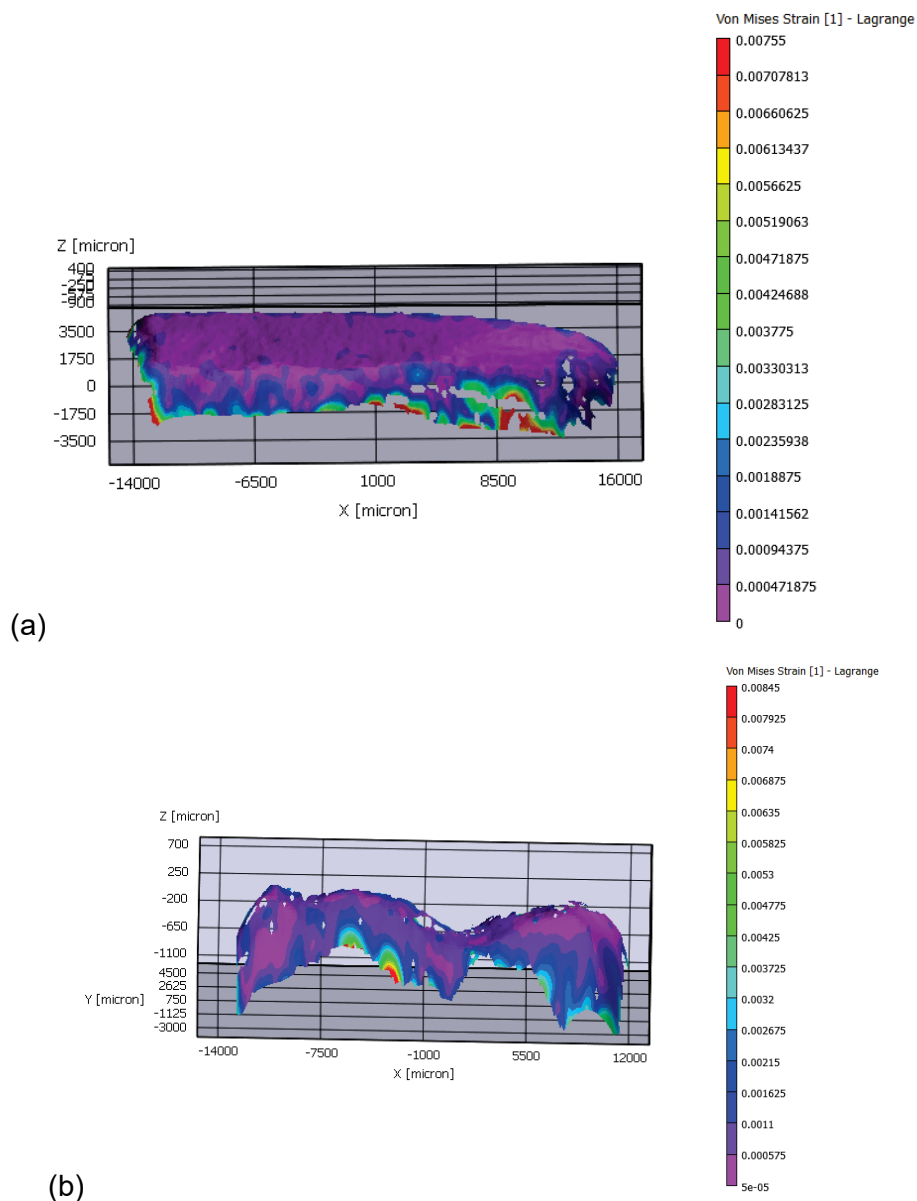


Figure 14. Representative image of the Vic-3D output for the distribution of the Von Mises strain distribution, when tightening insertion post n.1 with a 20N torque value. **(a)** SS; **(b)** RS.

Discussion

For the best of our knowledge, this is an original study addressing the evaluation of micro-movements and strain distribution on a SS and on a RS, during pre-load torque, using the method of 3D Digital Image Correlation (DIC-3D).

The study conducted is also a pilot study. This term can refer to feasibility studies or pre-testing of a certain instrument (20), in this case passivity tests using SS and RS.

This kind of study presents great advantages in the investigation field, once it allows the identification of potential practical problems that may occur in the following research procedure, such as: where it could fail, where it might not be followed, or if the methods or instruments are suitable for the purpose or not. On the other hand, pilot studies can induce the researcher to make inaccurate predictions or assumptions (20).

In our study, several limitations were present, mostly due to financial factors.

The first limitation we came across was the choice of acrylic resin in which to embed the three implants, in order to reproduce the intraoral situation.

In the literature, the use of an epoxy resin (4, 21) seems to be a more accurate material for reproducing the edentulous human mandible than the one used, depending on the type of epoxy resin chosen, some have mechanical properties similar to natural cortical bone (elastic modulus of 15GPa) (21) or trabecular bone (elastic modulus of 3GPa) (4).

Clelland et al. describe the use of a different material for fabricating a mandibular resin model: ABS transparent resin (DSM Somos, Elgin, IL, USA), which as an elasticity modulus of 2 GPa, approximately the same as cancellous bone elasticity values reported on the literature (1.507 GPa) (22).

Another study also reports the use of a polyurethane block (F 16; Axson Technologies, France) for this purpose, which is an isotropic materials with uniform elastic properties similar to that of natural bone, its elastic modulus is 3.6GPa while the human bone elastic modulus is 4.0-4.5GPa (23).

In our pilot study, the acrylic resin chosen was the Ivoclar ProBase Cold, which has an elasticity modulus less similar to human bone than the previously mentioned materials. However, we have to keep in mind that the same acrylic block was used for both SS and RS, eliminating in this matter any bias as if variation between groups in mechanical properties could result from the acrylic block.

It is also reported in the literature, the use of more anatomically correct acrylic resin models, in order to reproduce more precisely the total or partially edentulous mandible (21, 22, 24), instead of a block-shaped acrylic resin model.

Again, to mimic a realistic clinical scenario concerning the shape of mandibular jaw, angulated or tilted implants (25) could have been used in our pilot-study, instead of vertical and parallel implants.

Also, the fact that implant insertion posts were used for the construction of the superstructures, instead of using the appropriate implant abutment replicas for that purpose, was seen as another limitation of our pilot study.

On the other hand, implants with different diameters (two 4.3x13mm Screw-Line ConeLog® implants and one 3.8x13mm Screw-Line ConeLog® implant) were used in our study. This may be seen as an advantage, once it is usually reported on the literature the use of same diameter implants, which can sometimes not be the case in a real intra-oral situation.

As it was previously referred, obtaining passive fit is always the objective of executing an implant-supported prosthesis, however distortions may occur in several stages of the fabrication process: impression procedure, master cast producing, wax pattern fabrication, framework fabrication, definitive prosthesis fabrication and delivery of the definitive prosthesis, as there are many and demanding clinical and laboratory steps when it comes to rehabilitating using implant-supported prosthesis (9).

In fact, misfit occurs due to accumulation of distortions throughout the procedure of final prosthesis fabrication, which is named distortion equation. In theory, if the summation of this distortion equation was equal to zero, passive fit could be achieved (9).

In our study, in order to certify the accuracy of the master cast, thus avoiding future misfit of the implant-supported framework, it was necessary to verify if the position of the implant analogs in the master cast coincided with the implants in the acrylic resin block, which represented the patient's mouth (14). This was accomplished through direct visualization, as previously described.

In Figures 6(a) and 7(a) there is no discrepancy between the superstructures and the master cast, which allows us to conclude that no distortion was induced in the fabrication of SS and RS in the laboratory using this master cast.

The acrylic resin block in which the implants are embedded represents the intraoral situation. In Figures 6(b) and 7(b) it is possible to see that no visual maladjustment was present between SS or RS and the acrylic block or, if there was a microgap present it would be lower than 30µm.

In fact, a framework should be considered passive when there is simultaneous circular contact between all the prosthetic cylinders and their respective implant abutment (26), in this case, between the insertion post and the implant analogs of the master cast and implants embedded in the acrylic resin block. Such characteristic was verified for SS and RS through direct visualization or amplification using the magnifying loupes.

Literature reports methods for verifying the accuracy of the master cast, such as an Accuracy Verification Template (AVT), in a light-cured resin. This AVT is constructed on the master cast and posteriorly transferred to the implants in the patients' mouth and if the

framework remains intact, it means that the transfer technique used successfully maintained the components in its right position and an accurate master cast was produced, therefore the restorative procedure may continue (14).

On the other hand, if the AVT breaks or suffers distortion when transferred to the implants in the patients' mouth, it means that the master cast is inaccurate and a technique for reestablishing the master cast's accuracy should be the next step. So, the framework segments are separated and related intraorally, then the corrected AVT is moved from the patient's mouth and an accurate master cast is produced using the adequate transfers (14).

Likewise, to test the accuracy of the master cast and avoid the construction of misfit frameworks, Manzella et al. aimed to create an inexpensive, easy to make and to use device that could verify if the position of implant replicas of the definitive cast were correct (27).

In this *in vitro* study, this device was made of type IV dental gypsum and it was 8mm high and 3mm thick, once, on the contrary of what happened with 1 and 2mm thick devices, this value of thickness permitted the removable of the device from the impression without fracturing. This was posteriorly screwed onto the implants, following Jemt's protocol, and the fracture of the device meant that misfit was present. It was concluded that this device was able to detect misfit *in vitro* and outcomes were not influenced by operator's experience (27).

Similarly, in our pilot study, SS was constructed using a type IV gypsum die (GC Fujirock® EP type IV).

Since the master cast constructed by the laboratory was considered accurate, fracture of SS and RS did not occur at any steps of the protocol.

On the other hand, if the master cast was not accurate it would have been easier to find discrepancies using SS, once this material has limited transverse strength, poor resistance to fracture and a higher dimensional stability (although a slight expansion occurs) when compared to resin materials, which have better mechanical properties, more resistance to fracture, but greater dimensional changes (some shrinkage occurs) (28).

In fact, polymerization shrinkage of pattern resins is an important factor to take in account when fabricating an implant-supported prosthesis, since dimensional stability of the pattern resin chosen influences the accuracy of the rehabilitation.

Gibbs et al. conducted a study in which they compared the polymerization shrinkage of two autopolymerizing pattern resins, GC Pattern Resin (GC America) and DuraLay (Reliance Dental Mfg Co) with two more recent photopolymerizing pattern resins, Primopattern LC Gel (Primotec) and Primopattern LC Paste (Primotec), by using a stereomicroscope with digital camera and imaging software (Stream Basic, Olympus Soft Imaging Solution GmbH) (29).

The author found that volume percentage of total polymerization shrinkage (mean \pm standard deviation) for GC Pattern Resin was 5.07 ± 1.36 , DuraLay 5.72 ± 0.89 , Primopattern

LC Gel 5.42 ± 1.83 and Primopattern LC Paste 7.43 ± 0.62 . Concluding that all pattern resins showed shrinkage after setting and volumetric values of DuraLay, GC Pattern Resin and Primopattern LC Gel, were in the same range (5.07%-5.72%), whereas, Primopattern LC Paste exhibited the highest shrinkage values (7.43%) (29).

For our pilot-study, the pattern resin chosen was a self-curing acrylic resin Pattern Resin™ LS (GC America Inc., Illinois, USA), which, according to the literature, exhibits a low value of volumetric shrinkage, making it ideal for the accurate fabrication of implant-supported prosthesis (29).

Concerning the Sheffield Test, it is reported on the literature as a commonly used method in clinical practice to evaluate framework fit (30). This test is performed by lightly tightening one single screw at a distal position abutment, loosening the other screws, and then observing the other abutments for passive fit (31), verifying if a gap was created between the other abutment-implant interface. If the superstructure remains in position in the loosened abutments, it is said to have acceptable passive fit. On the other hand, if a misfit is present, the superstructure will be lifted when a single screw is tightened, creating a gap (30).

In our pilot-study, using the Sheffield Test no visual lifting of the superstructure was seen when only a single screw was tightened. However, radiographic analysis shows a microgap on radiographs S1 and R1, in which the insertion post on the proximal end position is lightly tightened and the other two insertion posts are loosened. These microgaps were measured with the ImageJ software and the values obtained were $67\mu\text{m}$ and $99\mu\text{m}$ for RS and SS, respectively, and were considered to be clinically acceptable, as suggested in the literature by Jemt et al. (10). Therefore we went ahead with the three-dimensional image correlation analysis.

The DIC-3D method used in our pilot-study had the advantage of providing not only quantitative, but also qualitative data for the entire surface of the testing specimens (22), allowing evaluation of 3D representative images of the micro-movements and strain distribution of SS and RS, during increasing torques on the three transformed axes (U, V and W).

Analyzing the obtained data, minimum and maximum registered values of micro-movement and Von Mises strains were always superior for RS when compared to SS. This is justified by the fact that gypsum stone type IV, used to fabricate SS, has a higher dimensional stability and higher susceptibility to fracture, whereas resin materials have more resistance to fracture but greater dimensional changes (28), being more resilient and therefore allowing a wider range of micro-movements to occur, as it is seen in our pilot-study.

In Table II, it is also exhibited that the overall higher micro-movement values for both SS and RS were registered in the W component. In U and V components, lateral and vertical

micro-movements, respectively, were restricted by the implants' position; whereas, in the W component, there is no obstacle in the antero-posterior direction, allowing a wider range of micro-movement values in this direction.

By observing the representative images of the Vic-3D it was possible to compare SS and RS for the micro-movements suffered in the components U, V and W.

In the U component (Figure 11), for both superstructures similar and almost symmetrical micro-movement patterns were found and the highest values registered are always the micro-movements in the right direction. This may result from the fact that the insertion posts are always tightened in the same sequence: starting by tightening insertion post n.1 with a 10N torque value, followed by tightening insertion post n.2 and then insertion post n.3, for the same torque value; the same sequence is repeated for a torque value of 20N. In other words, insertion post n.3, located in the right extremity, is always the last one being tightened, for both 10N and 20N torque value.

While lateral micro-movements of SS in the opposite directions (left and right) do not show a great difference between them, RS shows a micro-movement in the right direction with almost double the value that in the opposite direction.

Since both superstructures were fabricating using the same master cast, this can be interpreted as a false negative for the RS, or a sign of lack of passivity of this superstructure comparatively to SS, in which opposite micro-movements were almost the same.

This can be due to the fact that resin materials suffer greater dimensional changes, with polymerization shrinkage, than gypsum stone materials (28).

In fact, in a previously mentioned study comparing the polymerization shrinkage of different pattern resin materials, it was concluded that the percentage of total polymerization shrinkage for GC Pattern Resin, the same resin material used in our pilot-study, was 5.07%. Although this material had the lowest value of polymerization shrinkage compared to the autopolymerizing and photopolymerizing resin materials tested (29), this occurrence of dimensional changes can be sufficient for introducing distortion and misfit in an implant-supported prosthetic rehabilitation.

When it comes to using auto-polymerized acrylic resin for splinting impression techniques, some suggestion have been given that can also be applied in the fabrication of resin superstructures: using the smallest amount of material possible; sectioning, with a disk, the resin bars between the implant copings and then reconnecting them using the increment or bead-brushing technique (9); and the use of pre-fabricated acrylic resin bars (2).

Concerning the V component depicted in Figure 12, both superstructures show again a similar and almost symmetrical pattern of vertical micro-movements and, again as a result of the sequence of insertion post tightening, the maximum values are mainly registered in the right extremity of SS and RS.

While RS shows approximately the same values of vertical micro-movements in the opposite direction, SS exhibits a micro-movement in the downwards direction about 70% lower than the one in the upwards direction. This can result from the higher dimensional stability (28) and greater rigidity of gypsum stone material, when compared to resin materials, making the behavior of SS more similar to that of a definitive framework, since it is usually fabricated in a metallic material, which also shows higher rigidity values.

As seen in Figure 13, for W direction, both superstructures show a very heterogeneous pattern of antero-posterior micro-movement, with approximate maximum and minimum values and RS exhibits once again greater values of antero-posterior micro-movement than SS, due to the previously reported characteristics inherent to resin materials.

During tightening of implant post n.2 with a torque value of 10N, the left side of RS tends to move towards the cameras, while the opposite side tends to move away from the cameras. This may be explained by the fact that, in this step, insertion post n.1 is already tightened (with a 10 N torque value), while insertion post n.3 is only manually tightened.

When in the presence of a misfit superstructure, tensile, compressive and bending forces may be introduced into an implant-supported prosthesis, resulting in failure of the components and also transferring stress into the bone/implant interface (32).

In order to evaluate the effects of horizontal or vertical misfit between implant and bar framework, some studies resorted to the construction of 3D models to analyze the resulting stresses quantified as Von Mises strain distributions (32, 33).

The same was performed in our pilot-study using DIC-3D and the software Vic-3D 2012.

By observing Figure 15, representing the Von Mises strain distribution, the maximum value of Von Mises stress found for RS is greater than that of SS. This was expected to happen, given the higher resilience values of the resin materials.

Also, in RS there is a higher chance of appearing failure, because higher Von Mises stress is a strong indicator of that occurrence (32).

Both SS and RS show a homogeneous Von Mises strain distribution, with a tendency for accumulating tension in the inferior region of the superstructure and the area of the neck of the insertion posts, while strain values found on the superior region of both superstructures tend to zero.

This is consistent with the information reported in a study by Taylor et al., a Finite Element analyses conducted on an implant-supported bar in which maximum and minimum values of horizontal misfit were introduced. By analyzing the strain value simulations for maximum (83.3 μ m) and minimum (71.5 μ m) values of horizontal misfit, a symmetric stress distribution pattern was found and maximum stress values were localized in the inferior region of the bar and at the neck of the supporting implants (33).

Similarly, another study used a 3D FE model to evaluate the effect of different levels of vertical misfit between implant and bar framework and came across similar results. By analyzing the Von Mises stress distribution for increasing levels of vertical misfit, there was a tendency for concentration of the tensions in the retaining-screw neck, and implant platform and neck (32).

When interpreting the results obtained in our pilot-study, it is important to take in account the small number of samples used and the fact that it is an *in vitro* study.

More studies are necessary, with a larger group sample and ideal protocol conditions, such as the use of an anatomical epoxy resin model to reproduce the intraoral situation and the construction of SS and RS using the appropriate implant abutment replicas instead of implant insertion posts, in order to evaluate micro-movements and strain distribution on a SS and RS, on an implant-supported prosthesis, during pre-load torque, using the method of 3D Digital Image Correlation (DIC-3D).

Conclusions

Within the limitation of this pilot-study, it was possible to evaluate and compare SS and RS used for passivity tests on an implant-supported prosthesis, by analyzing micro-movements and strain distribution of both superstructures, using the method of 3D Digital Image Correlation (DIC-3D).

SS and RS exhibit similar patterns of micro-movement in the U, V and W components, as well as similar patterns in Von Mises strain distribution.

The followed tightening sequence influences the micro-movement and Von Mises strain distribution.

Comparing to SS, RS seems to be a worse superstructure for passivity tests, due to the higher values of micro-movement and strain distribution registered for this superstructure.

List of Figures

Figure 1	Implants maintained in place using two metallic rulers.
Figure 2	Implants embedded in acrylic resin.
Figure 3	Dual-phase one-step closed tray impression technique used. (a) Implants with the Impression posts; (b) Impression caps attached to the insertion posts; (c) Closed tray with the two silicones; (d) Final result of the impression technique with the retrieved impression caps and impression posts.
Figure 4	Master cast, fabricated in the laboratory.
Figure 5	Stone superstructure (SS) fabricated in the laboratory.
Figure 6	SS with all three insertion posts untightened: (a) Connected to the master cast; (b) Connected to the acrylic block.
Figure 7	RS with all three insertion posts untightened: (a) Connected to the master cast; (b) Connected to the acrylic block.
Figure 8	Radiographs of SS after manually screwing the superstructure to the implants embedded in the acrylic block: S1) X-ray with insertion post tightened on implant in position 1 (4.3 Ø, proximal end position) and the other two untightened; S2) X-ray with insertion post tightened on implant in position 2 (4.3 Ø, middle position) fully tightened and the other two untightened; S3) X-ray with insertion posts tightened on all implants.
Figure 9	Radiographs of RS after manually screwing the superstructure to the implants embedded in the acrylic block: R1) X-ray with insertion post tightened on implant in position 1 (4.3 Ø, proximal end position) and the other two untightened; R2) X-ray with insertion post tightened on implant in position 2 (4.3 Ø, middle position) fully tightened and the other two untightened; R3) X-ray with insertion posts tightened on all implants.

<p>Figure 10</p>	<p>Superstructures hand-sprayed with opaque white paint and air-sprayed with black paint using the Airbrush Pro-Color. (a) RS; (b) SS.</p>
<p>Figure 11</p>	<p>Representative image of the Vic-3D output for the micro-movements of the superstructures, considered the fixed rigid body removal, for the U direction, during tightening of implant post n. 2 with a torque value of 10N: (a) SS; (b) RS.</p>
<p>Figure 12</p>	<p>Representative image of the Vic-3D output for the micro-movements of the superstructures, considered the fixed rigid body removal, for the V direction, during tightening of implant post n. 2 with a torque value of 10N: (a) SS; (b) RS.</p>
<p>Figure 13</p>	<p>Representative image of the Vic-3D output for the micro-movements of the superstructures, considered the fixed rigid body removal, for the W direction, during tightening of implant post n. 2 with a torque value of 10N: (a) SS; (b) RS.</p>
<p>Figure 14</p>	<p>Representative image of the Vic-3D output for the distribution of the Von Misses strain distribution, when tightening insertion post n.1 with a 20N torque value. (a) SS; (b) RS.</p>

List of Tables

Table I	Characterization of the implants, impression copings, impression caps, insertion posts and implant analogues used. All the material produced by Camlog, Maybachstrasse, Germany.
Table II	Minimum and maximum values of micro-movement of SS and RS in the lateral (U), vertical (V) and antero-posterior (W) directions according to the torque applied to each implant insertion post. Individual values are expressed in micrometers (μm).

List of Abbreviations

FEM	Finite Element Analysis
SEM	Scanning Electron Microscopic Analysis
DIC	Digital Image Correlation
RS	Resin Superstructure
SS	Stone Superstructure
DIC-3D	3D Digital Image Correlation
V	Vertical
U	Lateral
W	Antero-Posterior
AVT	Accuracy Verification Template

Bibliographic References

1. Berejuk HM, Shimizu RH, de Mattias Sartori IA, Valgas L, Tiozzi R. Vertical microgap and passivity of fit of three-unit implant-supported frameworks fabricated using different techniques. *The International journal of oral & maxillofacial implants*. 2014;29(5):1064-70.
2. Monteiro DR, Goiato MC, Gennari Filho H, Pesqueira AA. Passivity in implant-supported prosthesis. *The Journal of craniofacial surgery*. 2010;21(6):2026-9.
3. de Castro GC, de Araujo CA, Mesquita MF, Consani RL, Nobilo MA. Stress distribution in Co-Cr implant frameworks after laser or TIG welding. *Brazilian dental journal*. 2013;24(2):147-51.
4. Karl M, Winter W, Taylor TD, Heckmann SM. In vitro study on passive fit in implant-supported 5-unit fixed partial dentures. *The International journal of oral & maxillofacial implants*. 2004;19(1):30-7.
5. Pesqueira AA, Goiato MC, Filho HG, Monteiro DR, Santos DM, Haddad MF, et al. Use of stress analysis methods to evaluate the biomechanics of oral rehabilitation with implants. *The Journal of oral implantology*. 2014;40(2):217-28.
6. de Aguiar FA, Jr., Tiozzi R, Rodrigues RC, Mattos Mde G, Ribeiro RF. An alternative section method for casting and posterior laser welding of metallic frameworks for an implant-supported prosthesis. *Journal of prosthodontics : official journal of the American College of Prosthodontists*. 2009;18(3):230-4.
7. Karl M, Graef F, Schubinski P, Taylor T. Effect of intraoral scanning on the passivity of fit of implant-supported fixed dental prostheses. *Quintessence international (Berlin, Germany : 1985)*. 2012;43(7):555-62.
8. Longoni S, Sartori M, Maroni I, Baldoni M. Intraoral luting: modified prosthetic design to achieve passivity, precision of fit, and esthetics for a cement-retained, implant-supported metal-resin-fixed complete denture. *Journal of prosthodontics : official journal of the American College of Prosthodontists*. 2010;19(2):166-70.
9. Buzayan MM, Yunus NB. Passive Fit in Screw Retained Multi-unit Implant Prosthesis Understanding and Achieving: A Review of the Literature. *Journal of Indian Prosthodontic Society*. 2014;14(1):16-23.
10. Jemt T. Failures and complications in 391 consecutively inserted fixed prostheses supported by Branemark implants in edentulous jaws: a study of treatment from the time of prosthesis placement to the first annual checkup. *The International journal of oral & maxillofacial implants*. 1991;6(3):270-6.
11. Mitha T, Owen CP, Howes DG. The three-dimensional casting distortion of five implant-supported frameworks. *The International journal of prosthodontics*. 2009;22(3):248-50.
12. Tiozzi R, Falcao-Filho H, Aguiar Junior FA, Rodrigues RC, Mattos Mda G, Ribeiro RF. Modified section method for laser-welding of ill-fitting cp Ti and Ni-Cr alloy one-piece cast implant-supported frameworks. *Journal of oral rehabilitation*. 2010;37(5):359-63.
13. Tahmaseb A, Mercelis P, de Clerck R, Wismeijer D. Optical scan analysis to detect minor misfit on implant-supported superstructures. *The International journal of oral & maxillofacial implants*. 2011;26(6):1344-50.
14. Swallow ST. Technique for achieving a passive framework fit: a clinical case report. *The Journal of oral implantology*. 2004;30(2):83-92.
15. Yamamoto E, Marotti J, de Campos TT, Neto PT. Accuracy of four transfer impression techniques for dental implants: a scanning electron microscopic analysis. *The International journal of oral & maxillofacial implants*. 2010;25(6):1115-24.
16. Ghanbarzadeh J, Dashti H, Karamad R, Alikhasi M, Nakhaei M. Effect of tightening torque on the marginal adaptation of cement-retained implant-supported fixed dental prostheses. *Dental research journal*. 2015;12(4):359-64.
17. Messias A, Rocha S, Calha N, Neto MA, Nicolau P, Guerra F. Effect of intentional abutment disconnection on the micro-movements of the implant-abutment assembly: a 3D digital image correlation analysis. *Clinical oral implants research*. 2015.

18. Tiozzi R, Vasco MA, Lin L, Conrad HJ, Bezzon OL, Ribeiro RF, et al. Validation of finite element models for strain analysis of implant-supported prostheses using digital image correlation. *Dental materials : official publication of the Academy of Dental Materials*. 2013;29(7):788-96.
19. McCormick N, Lord J. Digital Image Correlation. *Materials Today*. 2010;13(12):52-4.
20. van Teijlingen E, Hundley V. The importance of pilot studies. *Nursing standard (Royal College of Nursing (Great Britain) : 1987)*. 2002;16(40):33-6.
21. Abduo J, Bennani V, Lyons K, Waddell N, Swain M. A novel in vitro approach to assess the fit of implant frameworks. *Clinical oral implants research*. 2011;22(6):658-63.
22. Clelland NL, Yilmaz B, Seidt JD. Three-dimensional image correlation analyses for strains generated by cement and screw-retained implant prostheses. *Clinical implant dentistry and related research*. 2013;15(2):271-82.
23. de Vasconcellos DK, Kojima AN, Mesquita AM, Bottino MA, Ozcan M. A microstrain comparison of passively fitting screw-retained and cemented titanium frameworks. *The Journal of prosthetic dentistry*. 2014;112(4):834-8.
24. Tahmaseb A, van de Weijden JJ, Mercelis P, De Clerck R, Wismeijer D. Parameters of passive fit using a new technique to mill implant-supported superstructures: an in vitro study of a novel three-dimensional force measurement-misfit method. *The International journal of oral & maxillofacial implants*. 2010;25(2):247-57.
25. Dittmer MP, Nensa M, Stiesch M, Kohorst P. Load-bearing capacity of screw-retained CAD/CAM-produced titanium implant frameworks (I-Bridge(R)2) before and after cyclic mechanical loading. *Journal of applied oral science : revista FOB*. 2013;21(4):307-13.
26. Barbosa GA, das Neves FD, de Mattos Mda G, Rodrigues RC, Ribeiro RF. Implant/abutment vertical misfit of one-piece cast frameworks made with different materials. *Brazilian dental journal*. 2010;21(6):515-9.
27. Manzella C, Bignardi C, Burello V, Carossa S, Schierano G. Method to improve passive fit of frameworks on implant-supported prostheses: An in vitro study. *The Journal of prosthetic dentistry*. 2016.
28. Derrien G, Sturtz G. Comparison of transverse strength and dimensional variations between die stone, die epoxy resin, and die polyurethane resin. *The Journal of prosthetic dentistry*. 1995;74(6):569-74.
29. Gibbs SB, Versluis A, Tantbirojn D, Ahuja S. COMPARISON OF POLYMERIZATION SHRINKAGE OF PATTERN RESINS. *Journal of Prosthetic Dentistry*. 2014;112(2):293-8.
30. Eisenmann E, Mokabberi A, Walter MH, Freesmeyer WB. Improving the fit of implant-supported superstructures using the spark erosion technique. *The International journal of oral & maxillofacial implants*. 2004;19(6):810-8.
31. McDonnell T, Houston F, Byrne D, Gorman C, Claffey N. The effect of time lapse on the accuracy of two acrylic resins used to assemble an implant framework for soldering. *The Journal of prosthetic dentistry*. 2004;91(6):538-40.
32. Spazzin AO, Abreu RT, Noritomi PY, Consani RL, Mesquita MF. Evaluation of stress distribution in overdenture-retaining bar with different levels of vertical misfit. *Journal of prosthodontics : official journal of the American College of Prosthodontists*. 2011;20(4):280-5.
33. Winter W, Taylor TD, Karl M. Bone adaptation induced by non-passively fitting implant superstructures: a finite element analysis based on in vivo strain measurements. *The International journal of oral & maxillofacial implants*. 2011;26(6):1288-95.